JOURNAL OF GEOPHYSICAL RESEARCH, VOL. 112, D21101, doi:10.1029/2007JD008674, 2007

An observation-based formulation of snow cover fraction and its evaluation over large North American river basins

Guo-Yue Niu[1] and Zong-Liang Yang[1]

Received 19 March 2007; revised 30 May 2007; accepted 23 July 2007; published 1 November 2007.

[1] Snow cover strongly interacts with climate through snow albedo feedbacks. However, global climate models still are not adequate in representing snow cover fraction (SCF), i.e., the fraction of a model grid cell covered by snow. Through an analysis of the advanced very high resolution radiometer (AVHRR) derived SCF and the Canadian Meteorological Centre (CMC) gridded snow depth and snow water equivalent (SWE), we found that the SCF–snow depth relationship varies with seasons, which may be approximated by variations in snow density. We then added snow density to an existing SCF formulation to reflect the variations in the SCF–snow depth relationship with seasons. The reconstructed SCF with the gridded snow depth and SWE by employing this snow density–dependent SCF formulation agrees better with the AVHRR-derived SCF than other formulations. The default SCF formulation in the National Center for Atmospheric Research community land model (CLM), driven by observed near-surface meteorological forcings, simulates a smaller SCF and a shallower snow depth than observations. Implementation of the new SCF formulation into the NCAR CLM greatly improves the simulations of SCF, snow depth, and SWE in most North American (NA) river basins. The new SCF formulation increases SCF by 20–40%, decreases net solar radiation by up to 20 W m^{-2}, and decreases surface temperature by up to 4 K in most midlatitude regions in winter and at high latitudes in spring. The new scheme reproduces the observed SCF, snow depth, and SWE in terms of interannual variability and interbasin variability in most NA river basins except for the mountainous Columbia and Colorado River basins. It produces SCF trends similar to that of AVHRR. However, it produces greater decreasing trends in ablation seasons and smaller increasing trends in accumulation seasons than those of the CMC snow depth and SWE.

Citation: Niu, G.-Y., and Z.-L. Yang (2007), An observation-based formulation of snow cover fraction and its evaluation over large North American river basins, *J. Geophys. Res.*, *112*, D21101, doi:10.1029/2007JD008674.

1. Introduction

[2] Snow cover strongly interacts with climate through snow albedo feedbacks. Snow cover extent in late winter and spring in the Northern Hemisphere (NH) as monitored by the advanced very high resolution radiometer (AVHRR) has been decreasing since the middle 1980s in response to global warming [*Robinson and Frei*, 2000]. Reconstructed snow cover using in situ snow depth data also indicates a rapid reduction during melting season, especially in April since 1980s associated with the increased temperature [*Brown*, 2000]. On the other hand, the warming trend may be accelerated by decreases in snow cover through the positive snow albedo feedback. Over the midlatitude NH land areas, the strongest warming in February and March over the past 50 a is associated with extensive decreases in late winter snow accumulation [*Brown*, 2000]. Over Arctic regions, the summer warming mainly results from an increase in snow-free days and a decrease in snow cover due to the transition from short tundra to tall trees, masking more snow surfaces [*Chapin et al.*, 2005]. Snow cover also controls cold region hydrology. Snow mass accumulated in winter is critical for estimating springtime snowmelt and river flow, the freshwater input to the Arctic Ocean [*Yang et al.*, 2003]. Runoff from Arctic river systems constitutes about 50% of the net flux of freshwater into the Arctic Ocean [*Barry and Serreze*, 2000] and thus can affect ocean salinity, sea ice conditions, and hence the global thermohaline circulation.

[3] Over the past decade, land surface models (LSMs) for use in global climate models (GCMs) have experienced a transition from single-layer snow models to more complex multilayer snow models to accommodate more internal processes in snowpack, such as densification and multiphase changes of water [*Loth et al.*, 1993; *Lynch-Stieglitz*, 1994; *Sun et al.*, 1999; *Dai et al.*, 2003; *Yang and Niu*, 2003; *Xue et al.*, 2003]. Most of the multilayer snow schemes are simplified from schemes with detailed internal processes such as grain size growth and gravitational flows

[1]Department of Geological Sciences, John A. and Katherine G. Jackson School of Geosciences, University of Texas at Austin, Austin, Texas, USA.

0148-0227/07/2007JD008674$09.00

of liquid water within a snowpack [*Anderson*, 1976; *Jordan*, 1991]. These multilayer snow schemes have improved the simulation of snow depth and snow water equivalent in open, unvegetated areas at local scales. In addition, there have been developments in representations of radiative effects of the vegetation canopy [*Hardy et al.*, 1997; *Davis et al.*, 1997; *Yang and Friedl*, 2003; *Niu and Yang*, 2004; R. Essery et al., Radiative transfer modeling of a coniferous canopy characterized by airborne remote sensing, submitted to *Journal of Hydrometeorology*, 2007, hereinafter referred to as Essery et al., submitted manuscript, 2007] and hydrologic impacts of interception of snow by the vegetation canopy [*Storck et al.*, 2002; *Roesch et al.*, 2001; *Essery et al.*, 2003; *Gusev and Nasonova*, 2003; *Niu and Yang*, 2004]. Most of the developments are tested against in situ observations at local scales, and very few are implemented into GCMs. The enhancements in representing internal processes in snowpack and vegetation sheltering effects on mass and energy budgets of the underlying snow surface have improved snow simulations at local scales in both open and vegetated environments. However, snow depth varies greatly at subgrid scales of regional or global climate models because of heterogeneities in land cover, terrains, snow deposition, snowmelt, and meteorological conditions [*Liston*, 2004].

[4] In regional or global climate models, subgrid snow distributions are represented as snow cover fraction (SCF), i.e., the fraction of a grid cell covered by snow, through the relationship between SCF and snow depth. At a GCM grid cell scale, one of the largest uncertainties in modeling snow and its interactions with the atmosphere comes from SCF formulations and their associated parameters. Various SCF formulations as summarized in *Liston* [2004] result in a wide spread of SCFs. GCMs vary significantly in simulating SCF, and most of them underestimated SCF [*Frei and Gong*, 2005] because of unrealistic formulations. Most SCF formulations are parameterized as a function of grid cell mean snow depth and the ground roughness length. Some of them also considered the impacts of subgrid topography variations on SCF [*Douville et al.*, 1995]. Despite efforts in the development of SCF schemes over the past decade [e.g., *Yang et al.*, 1997; *Luce et al.*, 1999; *Liston*, 1999; *Mocko and Sud*, 2001; *Roesch et al.*, 2001; *Liston*, 2004], it is still problematic to represent SCF in GCMs because of limited data sets of snow depth at a GCM grid cell scale available for validating these schemes. However, *Brown et al.*'s [2003] high-quality gridded snow depth and snow water equivalent data sets provide us with an opportunity, for the first time, to examine existing SCF formulations and then reformulate SCF at a GCM grid cell scale.

[5] The National Center for Atmospheric Research (NCAR) community land model (CLM) describes snow physics in vertical directions in much more detail than subgrid snow distributions in horizontal directions, which is represented by SCF. Its unrealistic SCF formulation resulted in a biased climate. Various versions of the NCAR climate models (e.g., CCM3/LSM, CAM2/CLM2, and CAM3/CLM3) produced a warm bias in winter and spring over snow covered regions in both midlatitudes and high latitudes. *Dickinson et al.* [2006] attributed the warm bias in high latitudes to excessive downward longwave radiation emitted by excessive low clouds and unrealistic advection of heat from warmer sea surface driven by anomalously southerly winds. However, this did not fully explain the warm biases in midlatitudes in winter and high latitudes in spring.

[6] The main purposes of this study are (1) to examine several existing SCF formulations and reformulate SCF on the basis of data analyses and (2) to evaluate the multilayer physically based snow model in the NCAR CLM with the default and the reformulated SCF. We also assess the impacts of different SCF formulations on net solar radiation and surface temperature as well as the model's ability to simulate interannual variabilities and long-term trends in snow cover and snow depth.

2. Snow Model in the NCAR CLM

[7] A modified version of the NCAR CLM2 [*Bonan et al.*, 2002] is used in this study. The modifications include a frozen soil scheme that relaxes the dependence of hydraulic properties on ice content by introducing a fractional permeable area [*Niu and Yang*, 2006] and a simple groundwater model that represents the interactions of soil moisture and groundwater [*Niu et al.*, 2007].

[8] The snow model in the NCAR CLM is a multilayer physically based model [*Dai et al.*, 2003; *Oleson et al.*, 2004], which is primarily simplified from *Anderson* [1976] and *Jordan* [1991] by parameterizing gravitational liquid water flow and grain size growth while neglecting water vapor phase. The state variables for snow are partial volume of liquid water and ice, snow density (or depth), and temperature. The number of snow layers can be up to 5 depending on the total snow depth. Total snow mass is divided or combined at every time step in response to changes in layer depth because of snowfall, sublimation, and ablation while conserving energy and mass. The layer structure is to keep such a thin surface layer that the model can accurately resolve ground heat flux, which is critical for computing the energy available for ablation.

[9] Snow density is solved through three types of compaction processes: destructive metamorphism of new snow, i.e., crystal breakdown due to wind or thermodynamic stress; snow load or overburden; and melting, changes in snow structure due to melt-freeze cycles plus changes in crystals due to liquid water. The temperature profile is first computed without phase change and then readjusted for phase change. The readjustment involves three steps: (1) the temperatures are reset to the freezing point for layers undergoing phase change when the layer temperature is greater than the freezing point and the ice mass is not equal to zero (i.e., melting), or when the layer temperature is less than the freezing point and the liquid water mass is not equal to zero (i.e., freezing); (2) the rate of phase change is assessed from the energy excess (or deficit) resulting from adjusting the layer temperature to the freezing point; and (3) the ice and liquid mass and the layer temperature are readjusted. Water flow is computed by a simple explicit scheme that permits a portion of liquid water over the holding capacity of snow to percolate into the underlying layer. The water flow out of the bottom of the snowpack is then available for infiltration into the soil and runoff.

[10] Snow albedo, α_{sno}, adopted from BATS, is a function of snow age, grain size, solar zenith angle, impurity, and the amount of fresh snow [*Warren and Wiscombe*, 1980]. Over

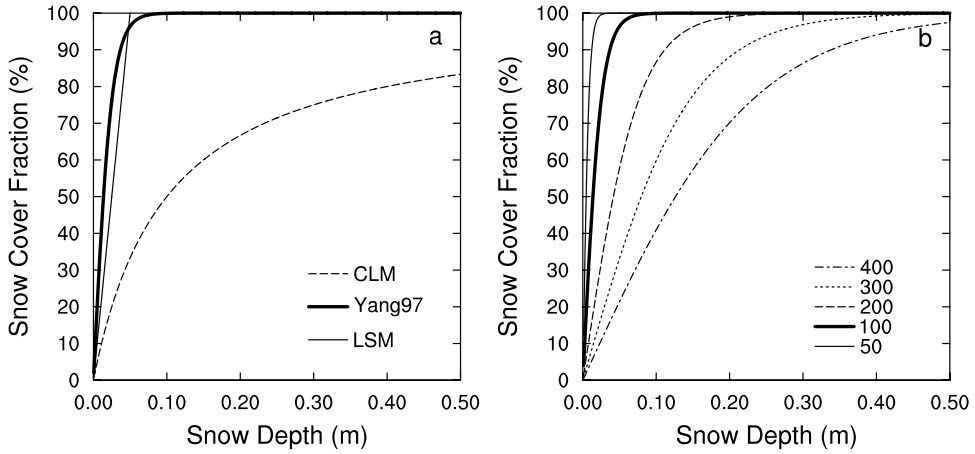

Figure 1. (a) SCF (or f_{sno}) computed from equation (2) (used in the default CLM and BATS), equation (3) of *Yang et al.* [1997], and a formulation used in the NCAR LSM1.0, $f_{sno} = \min(1, h_{sno}/0.05)$, where h_{sno} is snow depth (m) and (b) SCF as a function of ground surface roughness, snow depth, and snow density computed from equation (4) with new snow density $\rho_{new} = 100$ kg m^{-3} and $m = 1.6$. The thick line (i.e., $\rho_{sno} = 100$ kg m^{-3}) is equivalent to equation (3).

a snow-covered grid cell, ground surface albedo, α_g, is parameterized as an area-weighted average of albedos for snow (α_{sno}) and bare soil (α_{soi}):

$$\alpha_g = (1 - f_{sno})\alpha_{soi} + f_{sno}\alpha_{sno} \quad (1)$$

where f_{sno} is the fractional area of the grid cell covered by snow, or snow cover fraction. Adopted from BATS, f_{sno} is parameterized as a nonlinear function of snow depth, h_{sno} (in meters):

$$f_{sno} = h_{sno}/(10z_{0,g} + h_{sno}) \quad (2)$$

where $z_{0,g}$(= 0.01 m) is the ground roughness length. It shows a slower increment with snow depth than other formulations (Figure 1a).

[11] Surface albedo over a vegetated tile is solved through a two-stream approximation scheme for radiation transfer [*Dickinson*, 1983; *Sellers*, 1985] with ground surface albedo (α_g) as an input. Sky view factor as used in CLASS [*Verseghy*, 1991] and ECHAM4 [*Roesch et al.*, 2001] is not considered in the model to parameterize SCF and surface albedo, because the more complicated two-stream radiation transfer scheme already accounts for the sheltering effects of forests on underlying snow. The two-stream approximation also accounts for the effects of the canopy-intercepted snow on surface albedo by modifying vegetation optical properties. However, the two-stream approximation should be modified to account for within-canopy and between-canopy gaps [*Yang and Friedl*, 2003; *Niu and Yang*, 2004; *Pinty et al.*, 2006] induced by subgrid tree distributions at various scales (Essery et al., submitted manuscript, 2007) and clumping of needle leaves [*Chen et al.*, 1991].

3. Data Sets

[12] The data sets used in this study include atmospheric forcing, the National Oceanic and Atmospheric Administration (NOAA) AVHRR snow cover fraction, CMC snow depth and SWE, and U.S. Air Force/Environmental Technical Application Center (USAF/ETAC) snow depth climatology. Table 1 lists all the data sets used in this study.

3.1. Atmospheric Forcing [*Qian et al.*, 2006]

[13] This is a long-term (1948–2004) global surface meteorological data set at a T62 (~1.875°) resolution and a 3-h interval. The data set combined observation-based analyses of monthly precipitation and surface air temperature with intramonthly variations from the National Centers for Environmental Prediction–NCAR (NCEP-NCAR) reanalysis, which has spurious trends and biases in surface temperature and precipitation. Surface downward solar radiation from the reanalysis was first adjusted for variations and trends using monthly station records of cloud cover anomaly and then for mean biases using satellite observations during recent decades. Surface specific humid-

Table 1. Data Sets Used in This Study

Types	Duration	Spatial Resolution	Temporal Resolution	Author
atmospheric forcing	1948–2004	global T62	3 hourly	*Qian et al.* [2006]
snow cover fraction	1968–2002	NH 1°	monthly	*Robinson and Frei* [2000]
snow depth	1979–1996	NA 0.25°	daily	*Brown et al.* [2003]
SWE	1976–1996	NA 0.25°	daily	*Brown et al.* [2003]
USAF snow depth	climatology	global 1°	monthly	*Foster and Davy* [1988]
topography	static	global 1 km	static	Gtopo30

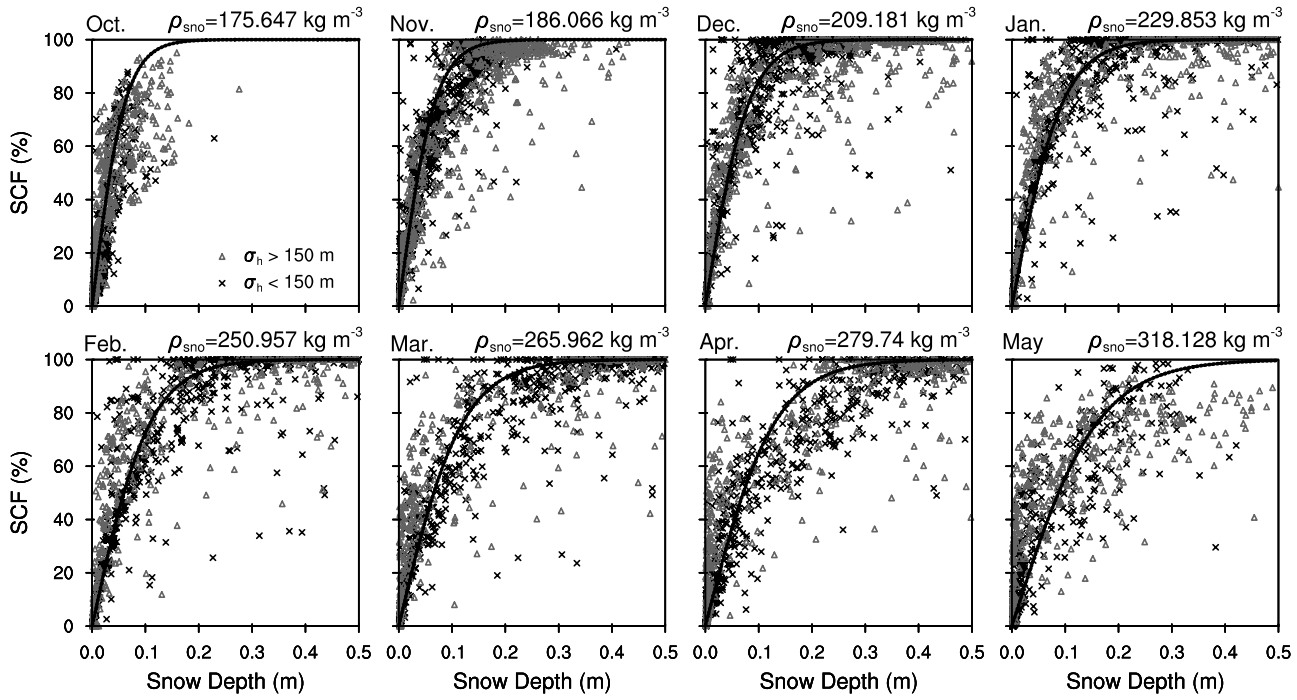

Figure 2. Relationship between AVHRR SCF (%) and CMC snow depth (m) in 1° × 1° grid cells of major NA river basins including the Mackenzie, Yukon, Churchill, Fraser, St. Lawrence, Columbia, Colorado, and Mississippi from October to May. The darker crosses stand for 1° × 1° grid cells where the standard deviation of topography σ_h < 150 m, and the lighter triangles stand for 1° × 1° grid cells where σ_h >150 m. The fitted lines are computed from equation (4) (m = 1.6) with the mean snow densities shown above each frame.

ity from the reanalysis was adjusted using the adjusted surface air temperature and reanalysis relative humidity. Surface wind speed and air pressure were interpolated directly from the 6-hourly reanalysis data. This data set was demonstrated to be of high quality through evaluations of model simulations against observed streamflow, continental freshwater discharge, and soil moisture [*Qian et al.*, 2006].

3.2. NOAA AVHRR Monthly SCF [*Robinson and Frei*, 2000]

[14] This NH long-term (1968–2003) monthly SCF data set at 1° × 1° resolution is averaged from weekly binary values computed from NOAA data by Rutgers University. The NOAA data [*Robinson*, 1993] consist of digitized weekly charts of snow cover derived from interpretation of visible satellite imagery by trained meteorologists. The data sets contain corrections recommended by *Robinson et al.* [1991] and the Rutgers weighting scheme to correctly partition weekly charts into appropriate months according to the number of days of a chart week falling in a given month [*Robinson*, 1993]. In general, the NOAA charts are considered to be the most accurate means of obtaining snow cover extent information on large regional to hemisphere scales. Furthermore, they comprise the longest satellite-based record available.

3.3. CMC Snow Depth and SWE [*Brown et al.*, 2003]

[15] These are daily snow depth and SWE at 0.25° resolution over North America (NA) for AMIP-2 (Second Atmospheric Model Intercomparison Project) period (1979–1996). The gridded snow depth combines in situ daily observations from ~8,000 U.S. cooperative stations and Canadian climate stations and first-guess fields with an optimum interpolation scheme developed by *Brasnett* [1999], which is employed operationally at CMC. The first guess fields were produced by a simple snow accumulation, aging and melt model driven by 6-hourly air temperature and precipitation from the European Centre for Medium-range Weather Forecasts (ECMWF) ERA-15 Reanalysis with extensions from the Tropical Ocean and Global Atmospheric Program (TOGA) operational data archive. The gridded snow depth and estimated SWE agreed well with available independent in situ and satellite data over midlatitude regions. The snow depth climatology exhibited several improvements over USAF/ETAC data, showing more realistic snow cover extents in fall and spring [*Brown et al.*, 2003; *Brown and Frei*, 2007]. While this data set is regarded as the currently best available estimates of large-scale snow depth and SWE over NA, the authors have the greatest confidence in the product in "data rich" areas of NA with relatively small orographic effects, which are mainly located east of the Rocky Mountains south of 55°N [*Frei et al.*, 2005].

3.4. USAF/ETAC Snow Depth Climatology [*Foster and Davy*, 1988]

[16] This data set is a monthly snow depth climatology. Snow depth is manually assigned, with varying confidence level, at 47 km NH polar stereographic grids according to

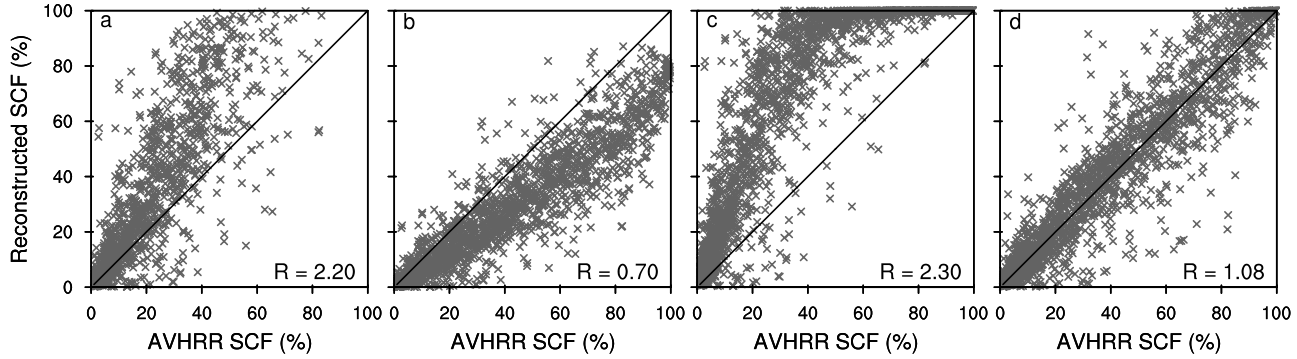

Figure 3. Reconstructed SCF using CMC snow depth and SWE with different SCF formulations. Plots are for (a) $f_{sno} = \min(1, h_{sno}/0.05)$, where h_{sno} is snow depth in meters; (b) equation (2); (c) equation (3); and (d) equation (4) with $m = 1.6$ in comparison with AVHRR SCF for all grid cells in the Mississippi River basin for all months. R is the averaged ratio of the reconstructed SCF to AVHRR SCF.

climatological records, literature searches, surface weather synoptic reports, and data obtained at snow course sites covering various time periods. In a number of countries, summarized snow depth values are not always available to construct a snow depth climatology with even a fair degree of confidence. Despite this limitation, a number of researchers used this data set to evaluate snow simulations [*Douville et al.*, 1995; *Foster et al.*, 1996; *Yang et al.*, 1999; *Roesch et al.*, 2001; *Roesch*, 2006; *Niu and Yang*, 2006]. Most recently, *Brown and Frei* [2007] pointed out evaluating GCM snow models with this data set may induce incorrect conclusions concerning the models' ability to simulate snowmelt and duration of snow seasons. In this study, we used it as a reference data set to see how it compares to CMC snow depth over various NA river basins.

4. Data Analyses: A New SCF Formulation

[17] To examine the relationship between snow cover fraction and snow depth and how this relationship may vary with seasons, we first aggregated the 0.25° CMC snow depth and SWE data sets into 1°, the same resolution as the AVHRR SCF. We then selected the CMC and AVHRR data sets during the same time period (1979–1996) to produce 1° climatologies of snow depth, SWE, and SCF. Then, we selected grid cells in eight major river basins (the Mackenzie, Yukon, Churchill, Fraser, St. Lawrence, Columbia, Colorado, and Mississippi), which include both mountainous and flat river basins and cover the most snow covered land area of NA.

[18] Figure 2 shows that the monthly relationship between the AVHRR SCF and the CMC snow depth varies from a more rapid increase in SCF with snow depth in earlier snow months (e.g., October, November, and December) to a slower increment in SCF with snow depth in melting months (e.g., March, April, and May). Meanwhile, snow density computed from the CMC snow depth and SWE averaged over the eight river basins shows a gradual increase from 176 kg m^{-3} in October to 318 kg m^{-3} in May.

[19] It is apparent that equation (2) or any other one-curve formulation cannot fit the observed SCF–snow depth relationship that is varying with seasons. *Yang et al.* [1997] found equation (2) underestimates SCF and surface albedo in local-scale simulations and reformulated f_{sno}:

$$f_{sno} = \tanh\left(\frac{h_{sno}}{2.5 z_{0,g}}\right) \tag{3}$$

Roesch et al. [2001] demonstrated the above equation is more applicable to flat, nonvegetated regions. As shown in Figure 1a, equation (3) results in a sharper increase in SCF with snow depth than does equation (2). However, it may overestimate snow cover fraction in melting season. Guided by Figure 2, we modified equation (3) to account for the variation of the SCF–snow depth relationship with season, which is represented by the variation in snow density, ρ_{sno}:

$$f_{sno} = \tanh\left(\frac{h_{sno}}{2.5 z_{0g}(\rho_{sno}/\rho_{new})^m}\right) \tag{4}$$

where snow density ρ_{sno} is scaled by the fresh snow density ρ_{new} (100 kg m^{-3} in this study), and m, a melting factor determining the curves in melting season, is adjustable depending on scale (generally, a larger value for a larger scale). It can be calibrated against observed snow cover fraction or surface albedo. In this study, it is estimated at ~1.6 as calibrated against the AVHRR SCF data. It is noteworthy that the prognostic snow density, ρ_{sno}, is the bulk density of the snowpack rather than that of the surface layer to produce a smoother SCF transition from accumulation seasons to melting seasons.

[20] Because the snowpack becomes much patchier in melting periods, it covers smaller areas than in snowfall periods given a same grid-averaged snow depth. This phenomenon is approximated in equation (4) through the variations in snow density. As shown in Figure 1b, during snowfall periods when snow density is relatively small, SCF increases more rapidly with snow depth than in melting periods when snow density becomes greater. As snowfall and ablation phases are mimicked by the bulk snow density,

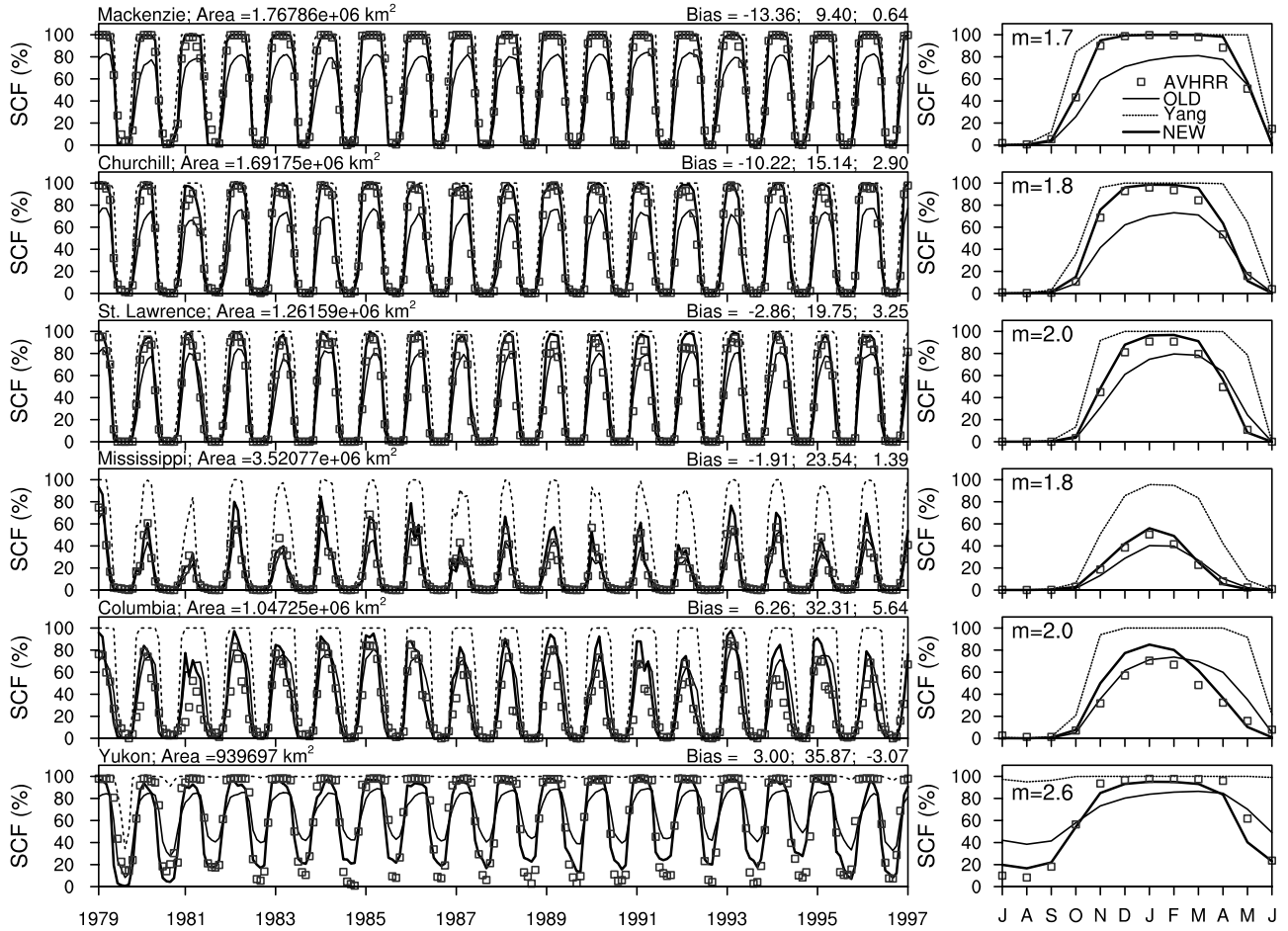

Figure 4. Reconstructed SCF using basin-averaged CMC snow depth and SWE with different formulations ("OLD" represents equation (2), "Yang" represents equation (3), and "NEW" represents equation (4) with optimized melting factors) in comparison with basin-averaged AVHRR SCF. The biases above each frame are for OLD, Yang, and NEW, respectively.

which varies smoothly with time, the transition of SCF from accumulation seasons to melting seasons is also gradual. Using the river basin averaged snow density for different months (shown above each frame of Figure 2), equation (4) (m = 1.6) matches very well to the observed SCF–snow depth relationship for a given month. Because the data quality in mountainous regions is not high enough, we did not see a clear dependence of the SCF–snow depth relationship on subgrid topography variations, which is represented by the standard deviation of topography, σ_h. For this reason, we did not further consider the impacts of subgrid topography on SCF into equation (4) as done by *Douville et al.* [1995] for their SCF formulations.

[21] Reconstructing snow cover using historical records of snow depth from stations is very important for investigating long-term snow cover variations and its correlations with climate change [*Frei et al.*, 1999; *Brown*, 2000]. A SCF–snow depth relationship is critical for reconstructing snow cover at either grid cell scales (Figure 3) or river basin scales (Figure 4). Figure 3 shows the reconstructed SCF for the $1^\circ \times 1^\circ$ grid cells in the Mississippi River basin using different formulations in comparison with the AVHRR SCF, where the CMC snow depth and SWE are considered of the best quality. It is clear that the default formulation in CLM (equation (2)) underestimated SCF and equation (3) overestimated SCF, while equation (4) (m = 1.6) matches the AVHRR SCF very well. Figure 4 shows the reconstructed SCF with different formulations using basin-averaged snow depth and SWE in comparison with the AVHRR basin-averaged SCF. Equation (4) with optimized melting factors for each river basin performs much better than equation (2) and equation (3) in capturing the AVHRR SCF on seasonal and interannual scales in various river basins. It appears that the optimum melting factor is smaller for plain river basins (e.g., the Mackenzie, Churchill, and Mississippi) than for mountainous river basins (the Columbia and Yukon) and greater at river basin scales than at grid cell scales (the Mississippi in Figure 4 versus Figure 3d). Optimization of the melting factor depending on topography and vegetation type is discussed in more detail by H. Su et al. (Enhancing the estimation of continental scale snow water equivalent by assimilating MODIS snow cover with the ensemble Kalman filter, submitted to *Journal of Geophysical Research*, 2007).

5. Model Results

[22] We conducted two experiments with the modified NCAR CLM2.0, one with the default SCF formulation

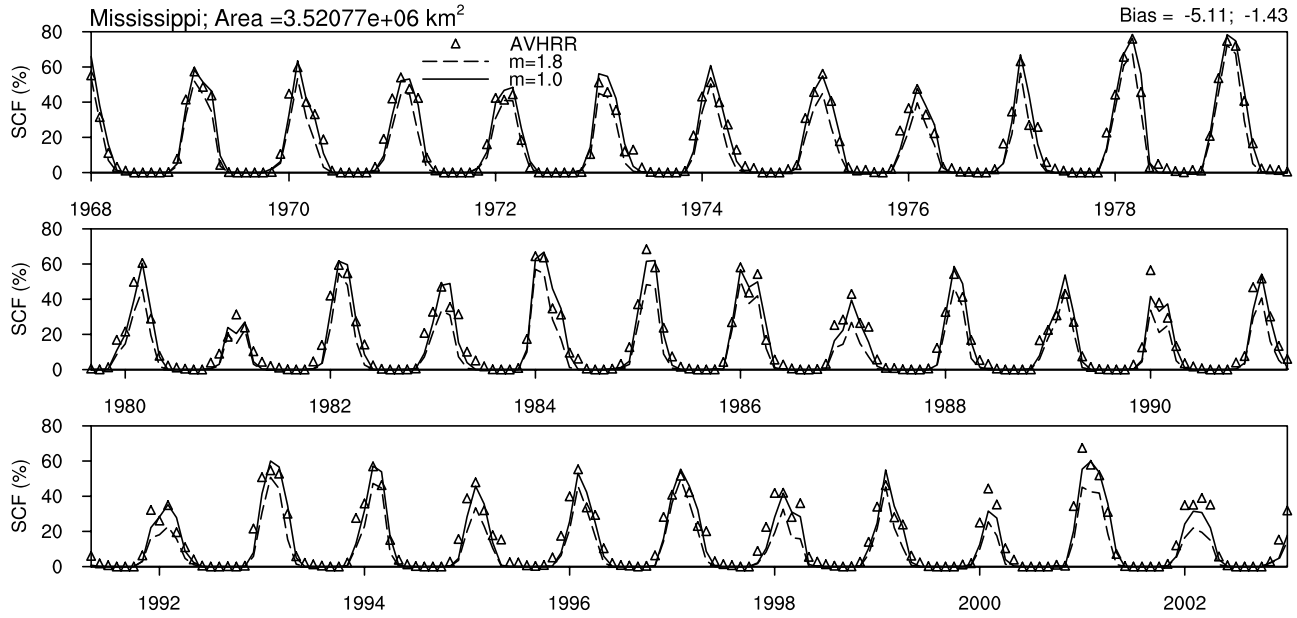

Figure 5. Modeled SCF using equation (4) with different melting factors (m = 1.0 and m = 1.8) in comparison with AVHRR SCF in the Mississippi River basin. The biases marked above the frame are for m = 1.8 and m = 1.0, respectively.

(equation (2)) and the other with the density-dependent SCF (equation (4)), driven by the near-surface atmospheric forcing data set [*Qian et al.*, 2006]. The two model runs were integrated from 1948–2002, while the model results during 1979–1996 were selected to compare to the AVHRR SCF and the CMC snow depth and SWE. The vegetation and soil parameters at T62 resolution were interpolated from the finer resolution raw data of the NCAR standard CLM2.0. The ground roughness length, which greatly affects SCF, is 0.01m in both experiments as in the standard CLM2.0.

[23] The melting factor in equation (4), m, equals 1.0 through sensitivity tests against the AVHRR SCF, a value smaller than the optimum values used for reconstructing SCF using the CMC estimates. This may be explained by the smaller 3-hourly time step at which the model is operated than the monthly scale at which the reconstruction was carried out. Ideally, the melting factor can be determined through data analyses given accurate data sets of snow depth, SWE, and SCF at the model's spatial and temporal resolution. However, these data sets do not exist so far, and thus calibration is required for both offline and coupled model runs. As shown in Figure 5, the modeled SCF with m = 1.0 shows a little improvement over that with m = 1.8 for the long-term SCF variations in the Mississippi River basin, as measured by biases.

[24] As shown in Figure 6, the density-dependent SCF (equation (4)) improves SCF simulations in all river basins in terms of interannual and interbasin variations over the default formulation (equation (2)). However, the model with the new formulation still meet difficulties in mountainous river basins, e.g., the Columbia, where the model underestimated SCF during the melting season, and the Colorado, where the model underestimated SCF in all seasons. The underestimation in mountainous river basins may be mainly attributed to the underestimated precipitation or snowfall due to gauge undercatch errors [*Adam et al.*, 2006; *Tian et al.*, 2007].

[25] The density-dependent SCF formulation produced greater snow depth (Figure 7) and SWE (Figure 8) in all the river basins than those with the default formulation. The modeled snow depth and SWE in most of the river basins are favorable compared to the CMC snow depth and SWE, except for those in the Churchill and North Central River basins. However, the degree of degradation in the modeled snow depth and SWE is negligible compared to errors in the atmospheric forcing data and uncertainties in representing other physical processes and their associated parameters in the model, such as densification processes, liquid water flow within the snowpack, radiation transfer through the vegetation canopy [*Niu and Yang*, 2004]. In addition, CLM does not explicitly account for sublimations from the canopy-intercepted snow and wind-blown snow, both of which can increase the surface area of snow exposed to the air and are thus conducive to an increase in sublimation, or radiation transfer through the snowpack, which can increase the absorption of solar radiation [*Flanner and Zender*, 2005].

[26] While the improvement in modeling SCF is observed in all the river basins including high-latitude river basins, the improvement in modeling snow depth and SWE by employing the density-dependent formulation is more obviously significant in midlatitude river basins. This may be explained by the greater incident solar radiation and thus a stronger snow albedo feedback in midlatitude river basins. Overall, the modeled snow depth by the NCAR CLM with the density-dependent SCF formulation agrees very well with the CMC data in terms of seasonality, interannual variability, and interbasin variability except for the mountainous Columbia and Colorado River basins.

[27] The modeled snow density (Figure 8) agrees well with CMC estimates, especially in snow accumulation

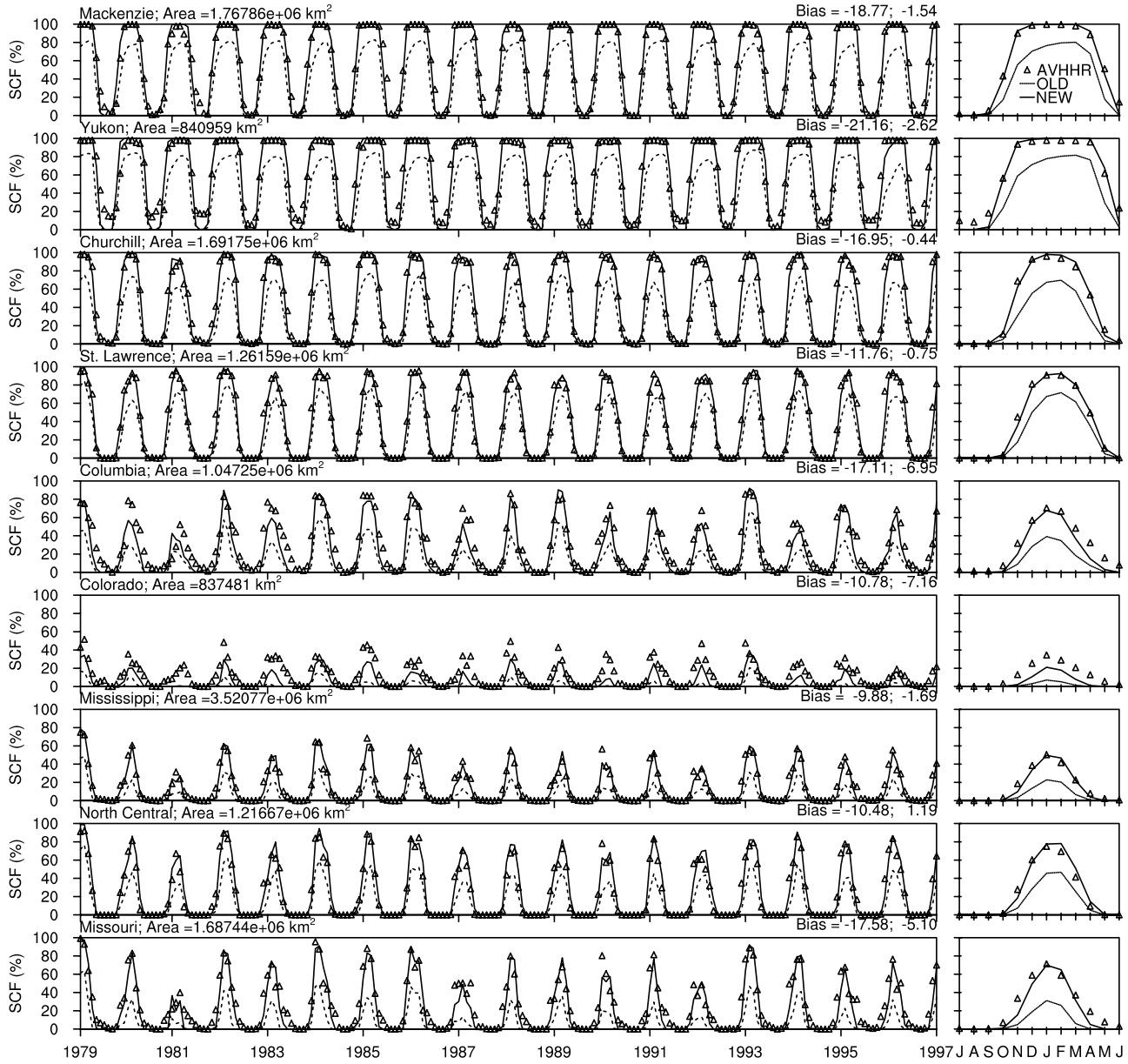

Figure 6. Modeled SCF in comparison with AVHRR SCF during 1979–1996 in various large NA river basins (m = 1.0 for the river basins). The smaller plots on the right show monthly averages of the 18-a data. The biases shown above each frame are for OLD and NEW, respectively.

season. It appears that different SCF formulations show no obvious impacts on the snow density simulation in most of the river basins. To derive the CMC SWE from snow depth observations, *Brown et al.* [2003] used a scheme for computing snow density. The scheme for accumulation seasons is the same as that used in CLM, and both were based on the work of *Anderson* [1976]. However, they differ for melting seasons. For such a reason, CLM-modeled snow densities are greater than those of CMC in melting season in almost all the river basins. Our previous offline tests using the Sleepers River data also revealed that the simple treatment on the compaction rate due to melting in CLM was a possible cause for the overestimated snow density in the melting season. Given the same amount of SWE, a greater snow density would produce a shallower snow depth, and in turn, a smaller SCF and surface albedo, and more solar energy absorbed by the ground, resulting in less SWE and snow depth as well as a shorter snow season. Additionally, snow density controls snowpack thermal conductivity [*Sturm et al.*, 1997]. Accurately modeling snow density in melting season is subject to further investigations in model developments.

[28] The density-dependent SCF formulation produced higher SCFs by up to 40%, and less net solar radiation by up to 20 W m^{-2}, and lower surface temperature by up to 4K in snow covered regions, mainly in midlatitudes in DJF, moving toward high latitudes in MAM (Figure 9). This reduction in surface temperature would be more significant in an online mode when coupled to atmospheric models [*Liston*, 2004], because, in the offline runs, the near-surface

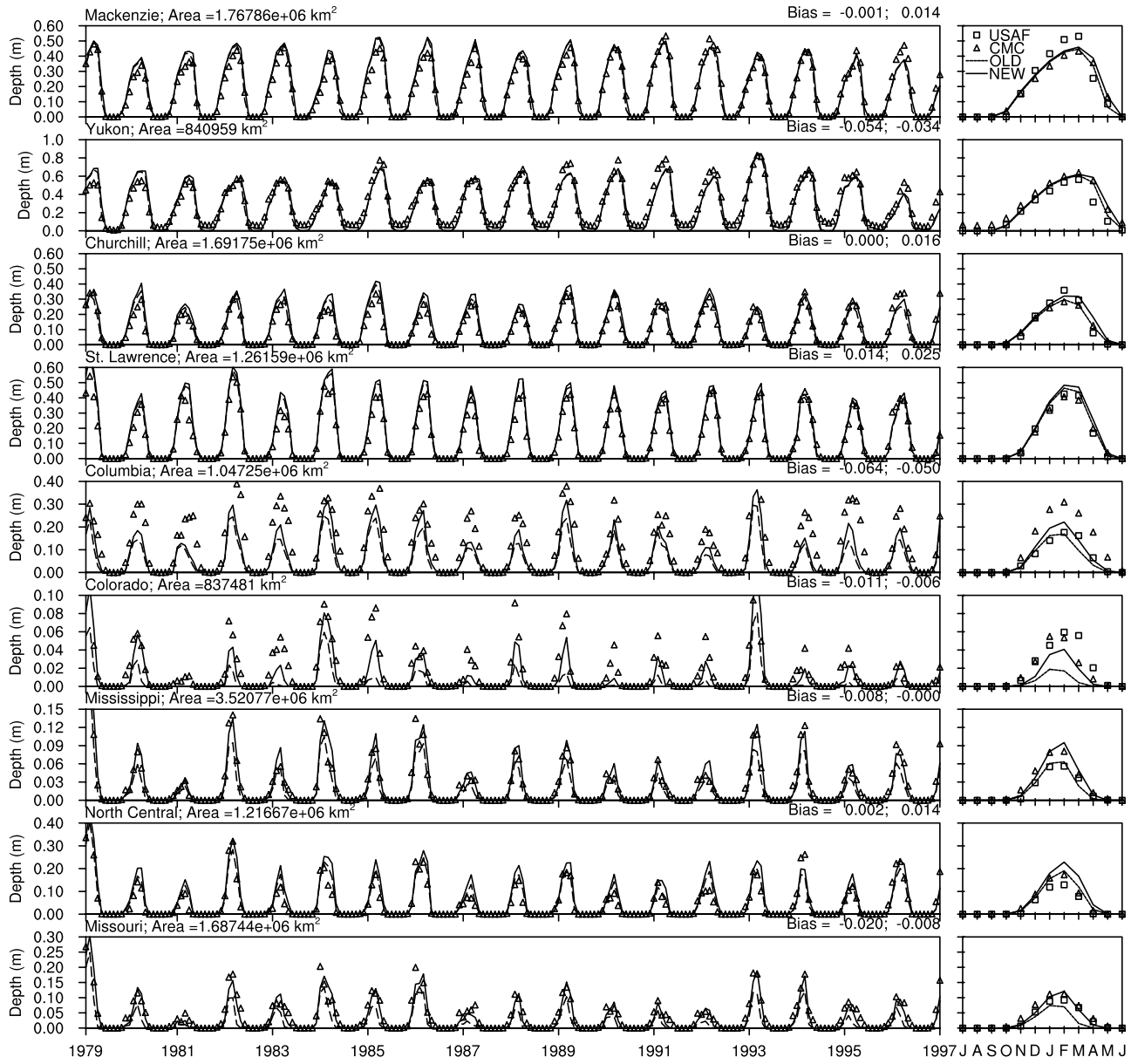

Figure 7. Same as Figure 6 but for modeled snow depth (m) in comparison with CMC data. The biases above each frame are for OLD and NEW, respectively.

air does not decrease with the cooler surface, thereby resulting in a spurious transfer of sensible heat fluxes to the cooler surface.

[29] Long-term snow cover variations can be seen as an indicator of climate change [*Robinson and Frei*, 2000]. Additionally, the strongest interactions between snow cover and climate usually occurs in spring months [*Brown*, 2000]. Therefore we also evaluated the model's ability to simulate long-term snow cover variations for each individual month over NA and Eurasia. As shown in Figure 10, the model performs very well in simulating the absolute values of the observed snow cover as well as the observed interannual variations and trends in snow cover in both NA and Eurasia except for November (and December in Eurasia). This is because snowfall, which is computed from precipitation using surface air temperature as a criterion, is more sensitive to the near-surface temperature in November, when the surface air temperature is more frequently around the criterion (for instance, 273.16 K) in most of the continents, than in other months. The modeled snow cover has higher correlations with the AVHRR in NA than in Eurasia, possibly because the new SCF formulation is developed against data sets in NA and the forcing data in NA have better qualities than those in Eurasia because of denser observation networks in NA. Both the model and AVHRR observation show decreasing trends in snow cover almost at the same rate in February, March, and April in both NA and Eurasia.

[30] The model performs very well in simulating the monthly mean values and interannual variabilities of snow depth and SWE (Figure 11) in large river basins over both NA and Eurasia. However, the model disagrees with CMC

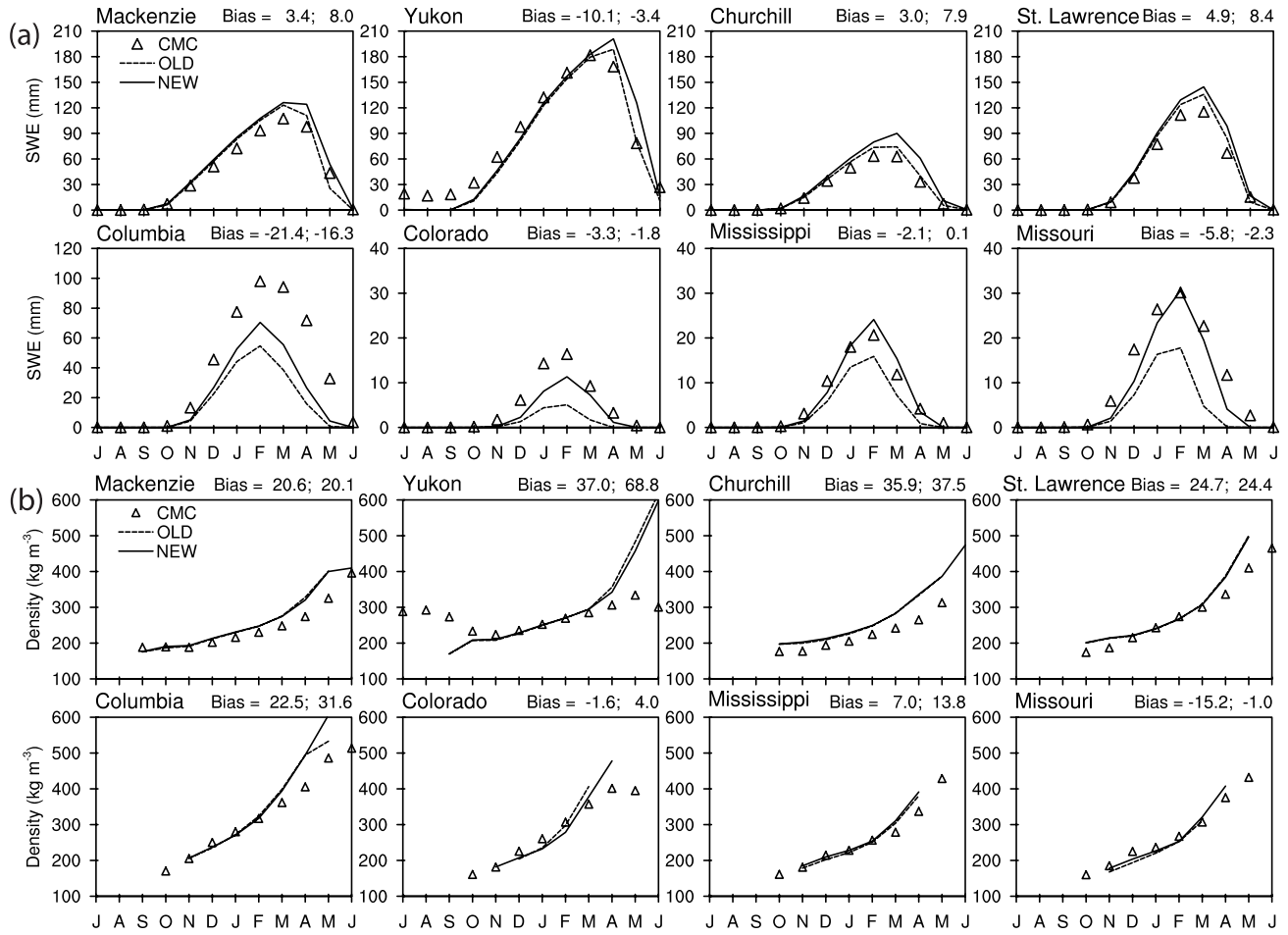

Figure 8. Comparison of modeled and CMC climatologies (monthly averages of 1979–1996 data) in eight large NA river basins. (a) SWE and (b) snow density. The biases above each frame are for OLD and NEW, respectively.

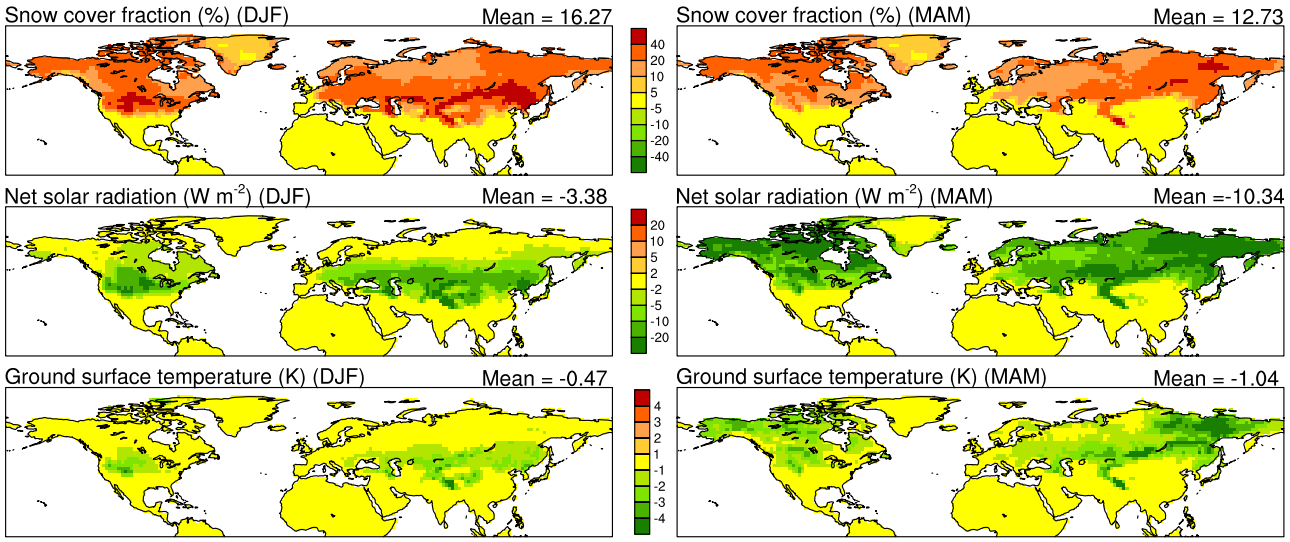

Figure 9. Modeled differences of SCF (%), absorbed solar radiation (W m^{-2}), and surface temperature (K) between the density-dependent formulation (equation (4)) and the default formulation (equation (2)) in DJF and MAM. The mean values above each frame are averages over all of the NH continents.

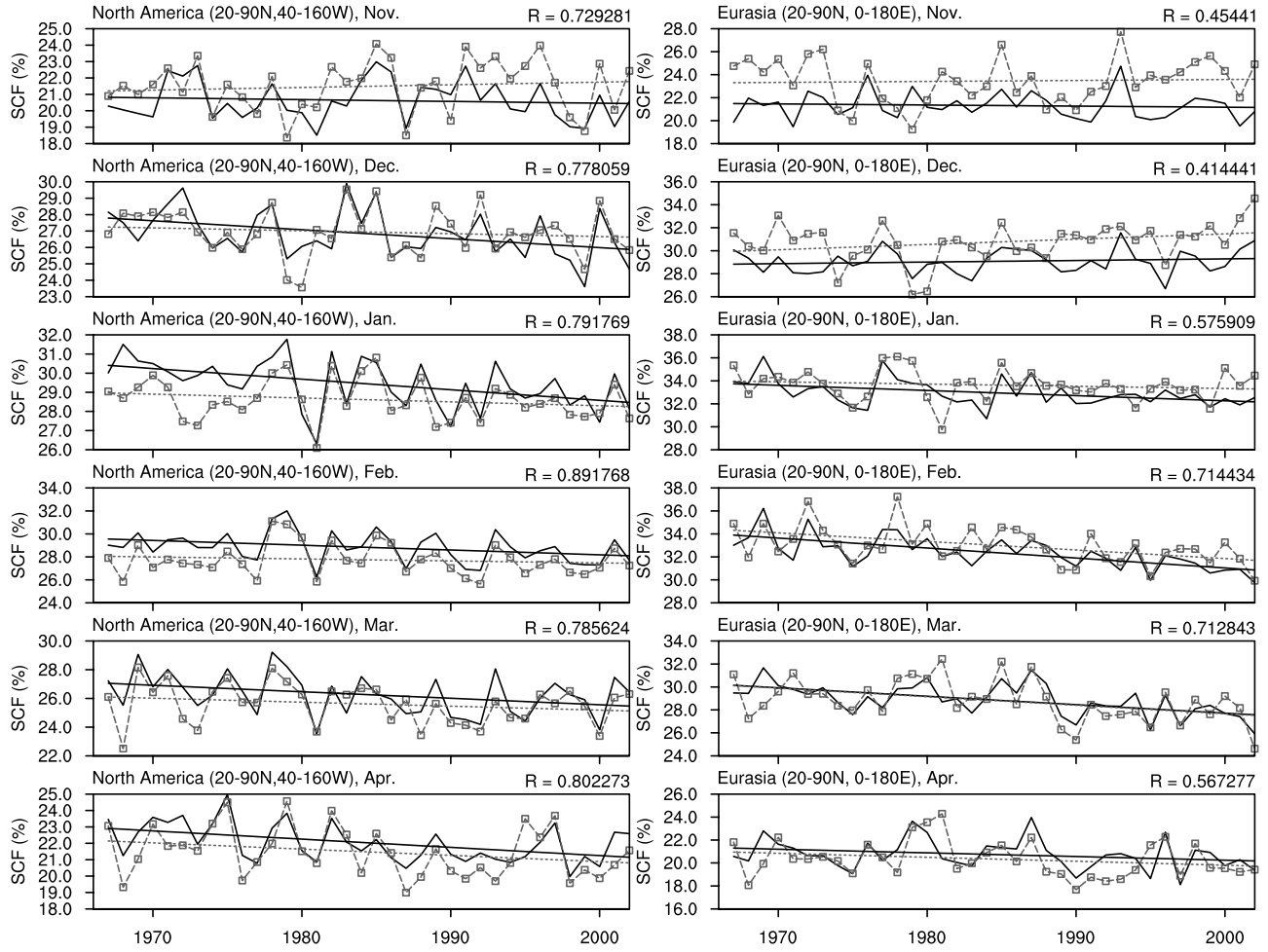

Figure 10. Modeled (thick solid lines) monthly SCFs and their trends in comparison with those of AVHRR data (thin dashed lines) averaged over NA (20°–90°N, 40°–160°W) and Eurasia (20°–90°N, 0°–180°N). Also shown on the top right corner of each plot are correlation coefficients (R) between the model and the AVHRR.

data in terms of trends in snow depth and SWE. Both CMC snow depth and SWE show increasing trends in snow accumulation season (November, December, and January), while the modeled snow depth and SWE show much slighter increasing trends in November and December and a decreasing trend in January. In snowmelt season (February, March, and April), the model shows much greater decreasing trends in both snow depth and SWE than do CMC estimates. This can be explained either by the CMC data quality, on which *Brown et al.* [2003] had higher confidence in the "data rich" regions east of the Rocky Mountains south of 55°N, or the model's lack of representation of some critical physical processes. Compared to the decreasing trend in AVHRR snow cover, CMC snow depth and SWE show no clear or weaker decreasing trend in February, March, and April. The inconsistency between AVHRR snow cover and CMC snow depth (SWE) warrants more attention in future studies. From the model aspect, CLM lacks a consideration of stability correction to the under-canopy aerodynamic resistance in vegetated regions, which may be a factor contributing to the snow climate feedback strength. In the melting season, turbulent sensible heat transfer from the warmer vegetation canopy to the cooler snow surface plays the same important role as absorption of solar radiation. This was also reflected by *Brown* [2000] that the largest decrease in snow cover occurred in April because of the warming trend. Stability correction to aerodynamic resistance can greatly suppress downward sensible heat flux from the warmer vegetation canopy, which absorbs solar radiation more efficiently than its underlying snow surface, to the cooler snow surface [*Niu and Yang*, 2004]. In addition, overestimation of snow density in melting season may also contribute to the stronger snow climate feedback by underestimating snow depth and hence snow cover given the same amount of SWE.

6. Summary

[31] We first analyzed the relationship between the AVHRR snow cover data and the CMC snow depth data and found it varies gradually from rapid SCF increments with snow depth in November and December to slower increases in April and May. We then added snow density to the *Yang et al.* [1997] SCF formulation to reflect the variations in the SCF–snow depth relationship with time.

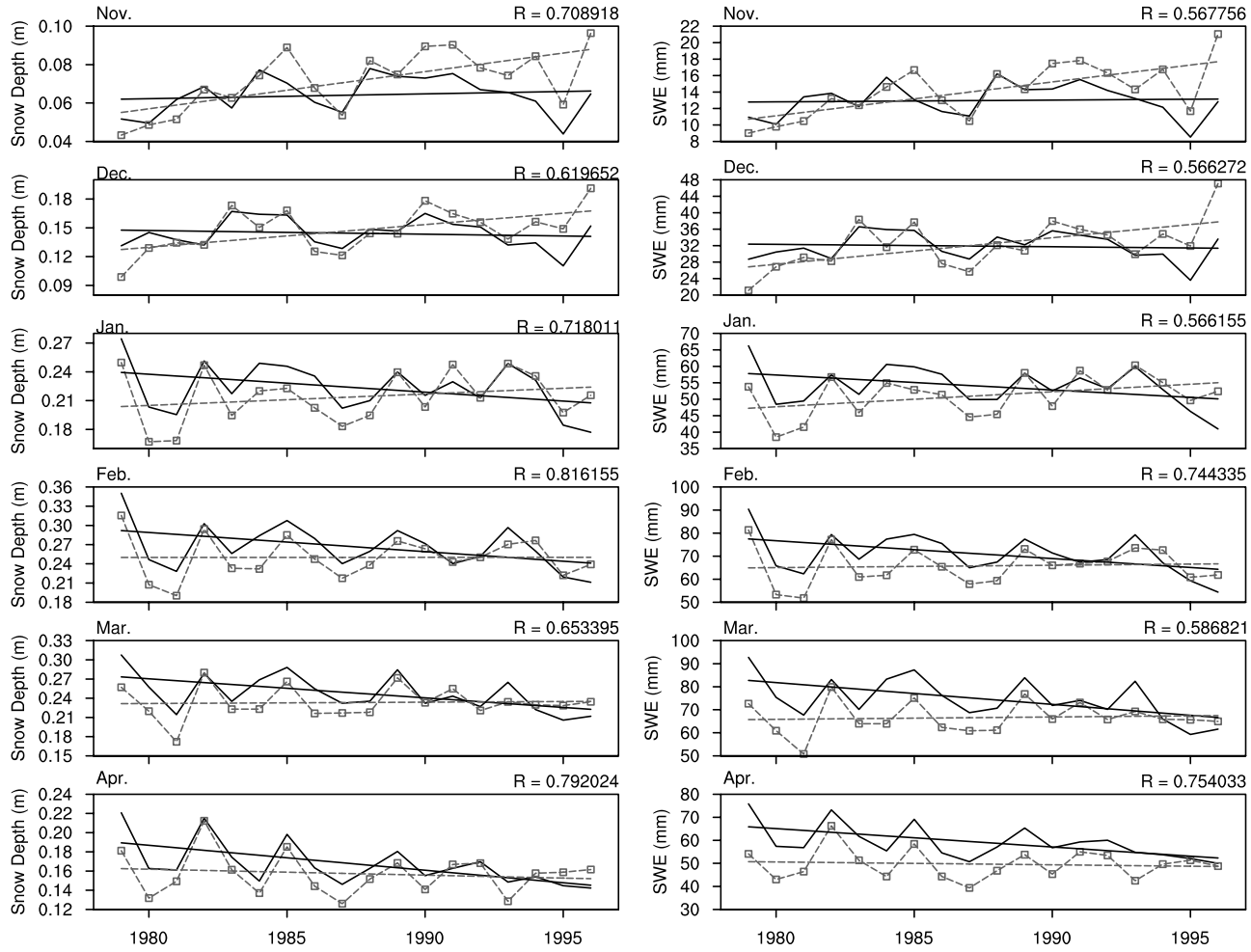

Figure 11. Modeled (thick solid lines) monthly (left) snow depth and their trends in comparison with CMC (thin dashed lines) snow depth and (right) SWE averaged over NA river basins north to 20°N. Also shown on the top right corner of each plot are correlation coefficients (R) between the model and the CMC.

The new snow density–dependent formulation agrees well with the observed SCF–snow depth relationship for each individual month and reconstructs AVHRR snow cover with the CMC snow depth and SWE data as inputs for the large NA river basins given optimized melting factors.

[32] When implemented into the NCAR CLM, the new SCF formulation (m = 1.0) greatly improved the simulation of SCF for all river basins as well as snow depth and SWE most obviously in midlatitude river basins. The new SCF formulation produced higher SCFs by up to 40%, and less net solar radiation by up to 20 W m^{-2}, and lower surface temperature by up to 4K in snow covered regions, mainly in midlatitudes in DJF, moving toward high latitudes in MAM. In wintertime, increases in snow cover fraction in midlatitudes induce more increments in SWE and snow depth than in high latitudes because of the greater solar radiation fluxes in midlatitudes.

[33] Overall, CLM with the new SCF formulation did a good job in simulating SCF, SWE, and snow depth in terms of seasonal, interannual, and interbasin variations except for mountainous river basins, where the snowfall is underestimated because of the gauge undercatch errors. CLM with the new SCF formulation also performed well in reproducing the decreasing trend in AVHRR SCF during melting season in both NA and Eurasia. The model produced a greater decreasing trend in snow depth and SWE than CMC data sets. This can be possibly explained by either the not-high-enough quality of CMC data sets or the lack of stability correction to the undercanopy aerodynamic resistance in CLM, which may result in a stronger snow climate feedback by overestimating the downward sensible heat transfer from the warmer vegetation canopy to its underlying snow surface in melting season. CLM also overestimates snow density in melting season because of the relatively simple treatment of densification formulation for snowmelt. This overestimation may also contribute to the stronger snow climate feedback by underestimating snow depth and hence snow cover given the same amount of SWE.

[34] **Acknowledgments.** This work was funded by NASA grant NNG04G061G, NAG5-12577 and NOAA grant NA03OAR4310076. Aiguo Dai and Taotao Qian are thanked for providing us with the atmospheric forcing data. Ross Brown is thanked for providing us with the CMC snow depth and SWE data. David Robinson is thanked for providing us with the AVHRR snow cover data. We also thank Keith

Oleson and other two anonymous reviewers for their constructive comments. The computing resources are provided by the Texas Advanced Computing Center (TACC).

References

Adam, J. C., E. A. Clark, D. P. Lettenmaier, and E. F. Wood (2006), Correction of global precipitation products for orographic effects, *J. Clim.*, *19*(1), 15–38.

Anderson, E. A. (1976), A point energy and mass balance model of a snow cover, *NOAA Tech. Rep. NWS 19*, 50 pp., Off. of Hydrol., Natl. Weather Serv. NOAA, Silver Spring, Md.

Barry, R. G., and M. C. Serreze (2000), Atmospheric components of the Arctic Ocean freshwater balance and their interannual variability, in *The Freshwater Budget of the Arctic Ocean*, edited by E. L. Lewis et al., pp. 45–56, Springer, New York.

Bonan, G. B., K. W. Oleson, M. Vertenstein, S. Levis, X. Zeng, Y. Dai, R. E. Dickinson, and Z.-L. Yang (2002), The land surface climatology of the community land model coupled to the NCAR community climate model, *J. Clim.*, *15*(22), 3123–3149.

Brasnett, B. (1999), A global analysis of snow depth for numerical weather prediction, *J. Appl. Meteorol.*, *38*, 726–740.

Brown, R. D. (2000), North Hemisphere snow cover variability and change, 1915–97, *J. Clim.*, *13*, 2339–2355.

Brown, R., and A. Frei (2007), Comment on "Evaluation of surface albedo and snow cover in AR4 coupled models" by A. Roesch, *J. Geophys. Res.*, doi:10.1029/2006JD008339, in press.

Brown, R. D., B. Brasnett, and D. Robinson (2003), Gridded North American monthly snow depth and snow water equivalent for GCM evaluation, *Atmos. Ocean*, *41*(1), 1–14.

Chapin, F. S., et al. (2005), Role of land-surface changes in Arctic summer warming, *Science*, *310*, 657–660.

Chen, J. M., T. A. Balck, and R. S. Adams (1991), Evaluation of hemispherical photography for determining plant area index and geometry of a forest stand, *Agric. For. Meteorol.*, *56*, 129–143.

Dai, Y., et al. (2003), The common land model (CLM), *Bull. Am. Meteorol. Soc.*, *84*(8), 1013–1023.

Davis, R. E., J. P. Hardy, W. Ni, C. Woodcock, J. C. McKenzie, R. Jordan, and X. Li (1997), Variation of snow cover ablation in the boreal forest: A sensitivity study on the effects of conifer canopy, *J. Geophys. Res.*, *102*, 29,385–29,389.

Dickinson, R. E. (1983), Land surface processes and climate-surface albedos and energy balance, in *Theory of Climate*, *Adv. Geophys*., vol. 25, edited by B. Saltzman, pp. 305–353, Elsevier, New York.

Dickinson, R. E., K. W. Oleson, G. B. Bonan, F. Hoffman, P. Thornton, M. Vertenstein, Z.-L. Yang, and X. Zeng (2006), The community land model and its climate statistics as a component of the community climate system model, *J. Clim.*, *19*(11), 2302–2324.

Douville, H., J.-H. Royer, and J.-F. Mahfouf (1995), A new snow parameterization for the Meteo-France climate model, part I: Validation in standalone experiment, *Clim. Dyn.*, *12*, 21–35.

Essery, R., J. Pomeroy, J. Parviainen, and P. Storck (2003), Sublimation of snow from coniferous forests in a climate model, *J. Clim.*, *16*(11), 1855–1864.

Flanner, M. G., and C. S. Zender (2005), Snowpack radiative heating: Influence on Tibetan Plateau climate, *Geophys. Res. Lett.*, *32*, L06501, doi:10.1029/2004GL022076.

Foster, D., and R. D. Davy (1988), Global snow depth climatology, *USAFETAC/TN-88/006*, 48 pp., U. S. Air Force Environ. Technol. Appl. Cent., Scott Air Force Base, Ill.

Foster, J., et al. (1996), Snow cover and snow mass intercomparison of general circulation models and remotely-sensed datasets, *J. Clim.*, *9*, 409–426.

Frei, A., and G. Gong (2005), Decadal to century scale trends in North America snow extent in coupled atmosphere-ocean general circulation models, *Geophys. Res. Lett.*, *32*, L18502, doi:10.1029/2005GL023394.

Frei, A., D. A. Robinson, and M. G. Hughes (1999), North American snow extent: 1900–1994, *Int. J. Climatol.*, *19*, 1517–1534.

Frei, A., R. Brown, J. A. Miller, and D. A. Robinson (2005), Snow mass over North America: Observations and results from the second phase of the Atmospheric Model Intercomparison Project (AMIP-2), *J. Hydrometeorol.*, *6*, 681–695.

Gusev, Y. M., and O. N. Nasonova (2003), The simulation of heat and water exchange in the boreal spruce forest by the land-surface model SWAP, *J. Hydrol.*, *280*, 162–191.

Hardy, J. P., R. E. Davis, R. Jordan, X. Li, C. Woodcock, W. Ni, and J. C. McKenzie (1997), Snow ablation modeling at the stand scale in a boreal jack pine forest, *J. Geophys. Res.*, *102*, 29397–29405.

Jordan, R. (1991), A one-dimensional temperature model for a snow cover, *CREEL Spec. Rep. 91-16*, Cold Regions Res. and Eng. Lab. U.S. Army Corps of Eng., Hanover, N. H.

Liston, G. E. (1999), Interrelationships among snow distribution, snowmelt, and snow cover depletion: Implications for atmospheric, hydrologic, and ecologic modeling, *J. Appl. Meteorol.*, *38*, 1474–1487.

Liston, G. E. (2004), Representing subgrid snow cover heterogeneities in regional and global models, *J. Clim.*, *17*, 1381–1397.

Loth, B., H.-F. Graf, and J. M. Oberhuber (1993), Snow cover model for global climate simulations, *J. Geophys. Res.*, *98*, 10451–10464.

Luce, C. H., D. G. Tarboton, and K. R. Cooley (1999), Sub-grid parameterization of snow distribution for an energy and mass balance snow cover model, *Hydrol. Processes*, *13*, 1921–1933.

Lynch-Stieglitz, M. (1994), The development and validation of a simple snow model for the GISS GCM, *J. Clim.*, *7*, 1842–1855.

Mocko, D. M., and Y. C. Sud (2001), Refinements to SSiB with an emphasis on snow physics: Evaluation and validation using GSWP and Valdai data, *Earth Interact.*, *5*, 1–31.

Niu, G.-Y., and Z.-L. Yang (2004), The effects of canopy processes on snow surface energy and mass balances, *J. Geophys. Res.*, *109*, D23111, doi:10.1029/2004JD004884.

Niu, G.-Y., and Z.-L. Yang (2006), Effects of frozen soil on snowmelt runoff and soil water storage at a continental scale, *J. Hydrometeorol.*, *7*(5), 937–952.

Niu, G.-Y., Z.-L. Yang, R. E. Dickinson, L. E. Gulden, and H. Su (2007), Development of a simple groundwater model for use in climate models and evaluation with GRACE data, *J. Geophys. Res.*, *112*, D07103, doi:10.1029/2006JD007522.

Oleson, K. W., et al (2004), Technical description of the community land model (CLM), *NCAR/TN-461+STR*, Natl. Cent. for Atmos. Res., Boulder, Colo.

Qian, T., A. Dai, K. E. Trenberth, and K. W. Oleson (2006), Simulation of global land surface condition from 19 48 to 20 04. part I: Forcing data and evaluations, *J. Hydrometeorol.*, *7*, 953–975.

Pinty, B., T. Lavergne, R. E. Dickinson, J.-L. Widlowski, N. Gobron, and M. M. Verstraete (2006), Simplifying the interaction of land surfaces with radiation for relating remote sensing products to climate models, *J. Geophys. Res.*, *111*, D02116, doi:10.1029/2005JD005952.

Robinson, D. A. (1993), Global snow monitoring: An update, *Bull. Am. Meteorol. Soc.*, *74*(9), 1689–1696.

Robinson, D. A., and A. Frei (2000), Seasonal variability of Northern Hemisphere snow extent using visible satellite data, *Prof. Geogr.*, *52*(2), 307–315.

Robinson, D. A., F. T. Keimig, and K. F. Dewey (1991), Recent variations in Northern Hemisphere snow cover, paper presented at 15th Annual Climate Diagnostics Workshop, NOAA, Asheville, N. C.

Roesch, A. (2006), Evaluation of surface albedo and snow cover in AR4 coupled climate models, *J. Geophys. Res.*, *111*, D15111, doi:10.1029/2005JD006473.

Roesch, A., M. Wild, H. Gilgen, and A. Ohmura (2001), A new snow cover fraction parameterization for ECHAM4 GCM, *Clim. Dyn.*, *17*, 933–946.

Sellers, P. J. (1985), Canopy reflectance, photosynthesis and transpiration, *Int. J. Remote Sens.*, *6*, 1335–1372.

Sturm, M., J. Holmgren, K. Konig, and K. Morris (1997), The thermal conductivity of seasonal snow, *J. Glaciol.*, *43*(143), 26–41.

Storck, P., D. P. Lettenmaier, and S. M. Bolton (2002), Measurement of snow interception and canopy effects on snow accumulation and melt in a mountainous maritime climate, Oregon, United States, *Water Resour. Res.*, *38*(11), 1223, doi:10.1029/2002WR001281.

Sun, S. F., J. M. Jin, and Y. Xue (1999), A simple Snow-Atmosphere-Soil Transfer (SAST) model, *J. Geophys. Res.*, *104*, 19587–19597.

Tian, X., A. Dai, D. Yang, and Z. Xie (2007), Effects of precipitation-bias corrections on surface hydrology over northern latitudes, *J. Geophys. Res.*, *112*, D14101, doi:10.1029/2007JD008420.

Verseghy, D. L. (1991), CLASS–A Canadian Land Surface Scheme for GCMs, part I: Soil model, *Int. J. Climatol.*, *11*, 111–133.

Warren, S. G., and W. J. Wiscombe (1980), A model for the spectral albedo of snow. II: Snow containing atmospheric aerosols, *J. Atmos. Sci.*, *37*, 2734–2745.

Xue, Y., S. Sun, D. S. Kahan, and Y. Jiao (2003), Impact of parameterizations in snow physics and interface processes on the simulation of snow cover and runoff at several cold region sites, *J. Geophys. Res.*, *108*(D22), 8859, doi:10.1029/2002JD003174.

Yang, D., D. Robinson, Y. Zhao, T. Estilow, and B. Ye (2003), Streamflow response to seasonal snow cover extent changes in large Siberian watersheds, *J. Geophys. Res.*, *108*(D18), 4578, doi:10.1029/2002JD003149.

Yang, R., and M. A. Friedl (2003), Modeling the effects of three dimensional vegetation structure on surface radiation and energy balance in boreal forests, *J. Geophys. Res.*, *108*(D16), 8615, doi:10.1029/2002JD003109.

Yang, Z.-L., R. E. Dickinson, A. Robock, and K. Y. Vinnikov (1997), Validation of the snow sub-model of the biosphere-atmosphere transfer

scheme with Russian snow cover and meteorological observational data, *J. Clim.*, *10*, 353–373.

Yang, Z.-L., and G.-Y. Niu (2003), The versatile integrator of surface and atmosphere processes (VISA) part 1: Model description, *Global Planet. Change*, *38*, 175–189.

Yang, Z.-L., et al. (1999), Simulation of snow mass and extent in general circulation models, *Hydrol. Processes*, *13*(12–13), 2097–2113.

G.-Y. Niu and Z.-L. Yang, Department of Geological Sciences, John A. and Katherine G. Jackson School of Geosciences, University of Texas at Austin, Austin, TX 78712-0254, USA. (niu@geo.utexas.edu)